HHS Public Access

Author manuscript

Brain Res. Author manuscript; available in PMC 2022 May 01.

Published in final edited form as:

Brain Res. 2022 May 01; 1782: 147840. doi:10.1016/j.brainres.2022.147840.

Extracellular vesicles released after cranial radiation: An insight into an early mechanism of brain injury

Suriyan Sukati[a,b,1], **Jenni Ho**[b,c,1], **Luksana Chaiswing**[b,c], **Pradoldej Sompol**[d], **Harshul Pandit**[b,c], **Wendy Wei**[e], **Tadahide Izumi**[b,c], **Quan Chen**[f], **Heidi Weiss**[c], **Teresa Noel**[b], **Subbarao Bondada**[c,g], **D. Allan Butterfield**[c,h], **Daret K. St. Clair**[b,c,*]

[a]Department of Medical Technology, Walailak Univeristy, Nakhon Si Thammarat, Thailand

[b]Department of Toxicology and Cancer Biology, University of Kentucky, Lexington, KY 40536, United States

[c]Markey Cancer Center, University of Kentucky, Lexington, KY 40536, United States

[d]Sanders-Brown Center on Aging, University of Kentucky, Lexington, KY 40536, United States

[e]Paul Laurence Dunbar High School, Lexington, KY 40513, United States

[f]Department of Radiation Medicine, University of Kentucky, Lexington, KY 40536, United States

[g]Department of Microbiology, Immunology, and Molecular Genetics

[h]Department of Chemistry, University of Kentucky, Lexington, KY 40536, United States

Abstract

Cranial radiation is important for treating both primary brain tumors and brain metastases. A potential delayed side effect of cranial radiation is neurocognitive function decline. Early detection of CNS injury might prevent further neuronal damage. Extracellular vesicles (EVs) have emerged as a potential diagnostic tool because of their unique membranous characteristics and cargos. We investigated whether EVs can be an early indicator of CNS injury by giving C57BJ/6 mice 10 Gy cranial IR. EVs were isolated from sera to quantify: 1) number of EVs using nanoparticle tracking analysis (NTA); 2) Glial fibrillary acidic protein (GFAP), an astrocyte marker; and 3) protein-bound 4-hydroxy-2-nonenal (HNE) adducts, an oxidative damage marker. Brain tissues were prepared for immunohistochemistry staining and protein immunoblotting. The results demonstrate: 1) increased GFAP levels ($p < 0.05$) in EVs, but not brain tissue, in the IR group; and 2) increased HNE-bound protein adduction levels ($p < 0.05$). The results support using EVs as an early indicator of cancer therapy-induced neuronal injury.

*Corresponding author at: Department of Toxicology and Cancer Biology, University of Kentucky, Lexington, KY 40536, United States. daret.stclair@uky.edu (D.K. St. Clair).

[1]Co-first authors.

Declaration of Competing Interest

The authors declare that they have no known competing financial interests or personal relationships that could have appeared to influence the work reported in this paper.

Appendix A. Supplementary data

Supplementary data to this article can be found online at https://doi.org/10.1016/j.brainres.2022.147840.

Keywords

Radiation; Extracellular vesicles; Oxidative stress; Lipid peroxidation

1. Introduction

Radiation therapy (RT) is a well-established and commonly used treatment for cancer patients because it effectively causes cancer cell death by targeting specific areas and minimizes undesired side effects in non-target tissues (Hall, 1973). However, despite treatment advances, damage to normal cells can cause serious, negative consequences; particularly, patients receiving cranial radiation can result in cognitive impairment (CI) as damage to healthy neurons is caused by cranial radiation, which negatively impacts patient quality- of- life. Therapy-induced CI causes alterations in learning, memory, behavior, and mood (Vitali et al., 2017). Neuronal damage is detected by neuroimaging techniques and neuropsychological evaluations (Cheung et al., 2016; Brinkman et al., 2018). Neuroimaging techniques, such as computed tomography, positron emission tomography, magnetic resonance imaging, and functional MRIs, detect structural and functional integrity of the brain, do not detect cellular level damage. Once neurobehavioral consequences resulting from cancer therapy have been detected, the efficacy of interventions declines (Cheung et al., 2016). As cognition remains altered long after the cessation of RT, the development of early indicators of neuronal damage would provide intervention capability.

The unique characteristics of extracellular vesicles (EVs) make them useful clinical tools: they are circulating, membrane-bound organelles released by nearly every cell in the body and contain molecular cargo that are protected from enzymatic degradation by a lipid bilayer (van Niel et al., 2018; EL Andaloussi et al., 2013). While the roles of EVs in normal and pathophysiological diseases have been extensively studied, the clinical use of EVs has only recently been appreciated (van Niel et al., 2018; Shah et al., 2018; Melo et al., 2014; Shao et al., 2012). We have demonstrated their potential as an earlier detector of cardiomyocyte damage following doxorubicin (DOX) treatment than the current standard method of measuring troponin levels (Vader et al., 2016; Yarana et al., 2018).

Ionizing radiation (IR) generates ROS, leading to increased oxidative damage (Hall, 1973). Under normal physiological conditions, reduction–oxidation (redox) regulation is tightly controlled by coordinating endogenous antioxidant systems (Baulch et al., 2016). The hydroxyl radical (•OH) can attack polyunsaturated fatty acids and initiate lipid peroxidation, making it an especially damaging free radical that IR generates (Dalleau et al., 2013). 4-hydroxy-2-nonenal (HNE) is a highly reactive product of lipid peroxidation and can covalently adduct to histidine, cysteine, or lysine residues of proteins through a Michael addition reaction or can form Schiff bases with the N-termini of peptide chains and the ε-amino groups of lysine residues of proteins (Dalleau et al., 2013; Butterfield and Halliwell, 2019). HNE adduction can cause protein misfolding and modify protein activity (Subramaniam et al., 1997).

Studies have demonstrated damage to the brain microenvironment caused by 10 Gy cranial radiation (Tomé et al., 2015; Baulch et al., 2016). Tomé et al., reported spatial memory

deficits in mice receiving whole brain radiation. Decreased neuronal cell proliferation and neurogenesis were observed in mice euthanized 48 h after receiving radiation, where these observations were further augmented in mice euthanized 8 days after radiation, establishing that consequences from cranial radiation are more difficult to detect immediately following the radiation compared to later (Tomé et al., 2015). We used the same animal model to determine the potential use of EVs as an early indicator of neuronal injury induced by cranial radiation. We analyzed oxidative stress and neuronal cell markers within EVs and compared them to brain tissue, identifying HNE-adducted proteins and glial fibrillary acidic proteins (GFAP) as EVs' cargos that increased early following cranial radiation. This study provides insights into biochemical markers of astrocyte activation and oxidative damage following cranial radiation and reveals the potential use of EVs as an early indicator of brain injury.

2. Results

2.1. Cranial radiation causes significant weight loss and increased levels of serum proteins

To monitor general radiation effects, we determined body weight, serum protein concentration, and serum HNE levels of male C57BJ/6 mice, which were given 10 Gy cranial radiation, the dose reported to cause cognitive impairment in mice and replicates effects seen in human patients who receive whole brain radiation treatment (Tomé et al., 2015; Baulch et al., 2016). Decrease in body weight of mice after radiation was statistically significant ($p < 0.05$) (Fig. 1A). Increase in serum protein concentration in the IR group was statistically significant compared to sham group ($p < 0.05$, Fig. 1B). No differences were observed in the amount of HNE- adducted proteins in the serum of the IR mice compared to the sham group ($p = 0.95$, Fig. 1C).

2.2. Radiation caused no significant differences in GFAP or HNE in brain tissue

Mice brains were removed and separated sagitally. The brain half that was to be homogenized was first separated into the hippocampus and cortex for quantification of GFAP. The two groups showed no significant difference in the amount of GFAP in brain tissue lysate (Fig. 2A). Each tissue slice of the hippocampus, which plays a role in new memory formation, was used for quantification, which considered brain tissue heterogeneity. The two groups showed no significant statistical difference in IHC staining of HNE (Fig. 2B). IHC measurement of GFAP in brain tissue was not significantly different (Fig. 2C).

2.3. Radiation- induced differences in astrocyte marker and oxidative stress are detectable in EVs

EVs isolated from mouse sera were evaluated for protein concentration differences (Fig. 3A) and for the number of EVs particles released by the two groups, utilizing nanoparticle tracking analysis (NTA) (Fig. 3B); the two groups showed no significant differences in EVs protein concentration or in the number of EVs particles observed. However, when the comparison of vesicle counts between the IR versus sham groups was adjusted for vesicle size, there was a significant difference between the two groups ($p < 0.05$); specifically, the difference between groups is evident and dependent according to vesicle

size (Supplementary Fig. A) which is corroborated by seeing a significant interaction term ($p < 0.01$) between group and vesicle size in the analysis model. To evaluate the amount of oxidatively modified proteins in the EVs, the EVs were lysed and measured for HNE adductions by HNE immunoblotting. Unlike both mice brain tissue and serum, HNE adducted proteins showed a statistically significant increase in the EVs isolated from the radiation-treated mice compared to the control (Fig. 3C, $p < 0.05$). A significant increase was consistently detected in the amount of GFAP in EVs from the IR mice compared to the sham group (Fig. 3D, $p < 0.01$).

3. Discussion

Cancer therapy-induced cognitive impairment is a serious side effect seen in cancer survivors. Neuroimaging and neuropsychological evaluations, the standard methods currently used to detect brain alterations associated with neurocognition decline, are limited and do not detect neuronal damage early enough for intervention to occur that would mitigate consequences (Cheung et al., 2016; Brinkman et al., 2018). In this study, we assessed whether markers of brain injury could be detected earlier in serum EVs than in brain tissue, utilizing radiation exposure as a model. Our results demonstrate that within 48 h following radiation treatment, radiation-induced brain injury, indicated by elevated levels of HNE-adducted proteins and radiation-induced an increase in GFAP, are detectable in EVs. Other potential markers of neuronal damage (NSE) and neuronal genesis (BDNF) were quantified in both homogenized brain tissue and EV lysates, but resulted in no statistical significance between the two groups (Supplementary Fig. B–E). This work suggests EVs are an early indicator of alterations to the brain microenvironment following cranial radiation. The results are consistent with our previous studies showing the levels of HNE-adducted proteins in mitochondrial lysates of animals treated with doxorubicin are increased nearly two-fold (Yarana et al., 2018). Importantly, this method provided earlier detection than the standard method of measuring cardiac troponin levels does (Dalleau et al., 2013). Therefore, our findings support a potential role of EVs as an early indicator of damage to the brain following toxic insults to the brain.

While we did not detect significant changes in biochemical markers in brain lysates or immunohistochemical analysis of brain tissues, we observed a trend of increase in those markers (Fig. 2). These observations are also consistent with previous studies that demonstrate how changes in neuronal generation and microglia activation were minor at 48 h after radiation treatment (Tomé et al., 2015). One potential mechanism leading to this observed difference between the increase in GFAP measured in the EVs and GFAP in the brain tissue could be a compensatory mechanism to dispose of oxidatively modified proteins due to the cranial radiation. It has been shown that EVs are being used to remove oxidatively modified proteins from the brain (Zhang, 2018). Thus, it is possible that the observed increase in GFAP in EVs but not in the brain tissue between the two groups is due, in part, to increased removal of oxidatively modified proteins by EVs.

The presence of HNE-adducted proteins in EV lysates also implicates a mechanism of tissue injury because HNE is a highly reactive end product of lipid peroxidation. The consequences of oxidative stress, and notably HNE, on the progression of neurodegenerative disorders

have been extensively reviewed (Lovell and Markesbery, 2007; Sultana et al., 2010; Perluigi et al., 2012; Di Domenico et al., 2017). The role of oxidative stress, indicated by the level of HNE, on declining neurocognition substantiates that EVs containing HNE-adducted proteins are valuable indicators of tissue damage.

GFAP, a marker of reactive astrocytes, which is activated by injury to the brain and has been shown to be increased in a variety of CNS disorders and neurodegenerative diseases, such as Alzheimer's disease (Chatterjee et al., 2021; Middeldorp and Hol, 2011), was also significantly increased. Finding GFAP increased in EVs but not in brain tissue further corroborates the benefit of using EVs as an early and more sensitive indicator than tissue histology of potential progression of neuro-degeneration. The increase of GFAP and HNE observed in the EVs, but not detectable in either mice brain tissue or serum, may be a result of the EVs protecting their molecular content from proteolytic degradation prior to EVs release or while in circulation. Because HNE is highly reactive, exposure to other cellular components in circulation may provide more challenges to quantifying HNE-adducted proteins in serum compared to EVs, where HNE-adducted proteins remain stable.

We and others have previously demonstrated the role of oxidative stress and inflammation in neurodegenerative diseases and cancer therapy-induced cognitive impairment (Keeney et al., 2018). Possibly, the observed increase in HNE-adducted proteins in EVs could potentially contribute to inflammation. Inflammatory cytokines such as TNF-α have been shown to induce reactive astrocytes, which could cause the increased expression of GFAP observed in this study (Hyvarinen, 2019; Tangpong, 2006; Tangpong et al., 2007; Chen et al., 2007; Aluise, 2011; Sompol et al., 2008). However, extensive cause/effect relationship studies will be needed to support this proposed link.

In summary, the present study demonstrates the benefit of using EVs as an early marker of brain damage following treatment with a dose of cranial radiation that has been documented to cause long-term neuro-anatomical alterations. Our results highlight the significance of changes in the markers of oxidative stress and glial cell activation observed in EVs prior to structural changes in brain tissue. Importantly, these tests can be performed using small amounts of available mice serum, suggesting the study is applicable to situations where only small amounts of blood are available. A limitation of the study is GFAP is not only present in brain cells but is also expressed in other tissues, particularly, cancer tissues. However, since the animals used did not have any cancer, this limitation does not detract from the observation that EV cargos are an early indicator of alterations to the brain microenvironment and are potential indicators of cancer therapy-induced cognitive impairment.

4. Experimental procedure

4.1. Animals and treatment

Male C57BL/6J mice 10–12 weeks old and 25–28 g body weight were housed at the University of Kentucky (UK), following the American Veterinary Medical Association Guidelines for the Care and Use of Laboratory Animals; UK's Institutional Animal Care and Use Committee approved their use. Ketamine at 100 mg/ml (Henry Schein, Inc.) with

Xylazine at 20 mg/ml (Akorn, Inc.) diluted in saline were used as anesthesia prior to cranial radiation treatment. Irradiated mice received one dose of 10 Gray cranial radiation using the X-ray irradiator, X-RAD 225XL, Precision X-ray (PXi), Inc. (225 kVp peak voltage, 0.3 mm Cu filtration, and 0.92 mm Cu beam quality). The irradiator was calibrated with in-air method following American Association of Physicist in Medicine TG-61 protocol (Ma et al., 2001) with an ADCL calibrated A1SL ion chamber (Standard Imaging Inc.) (Chen et al., 2021). Radiation field was set at 1.41 by 1.2 cm with field light guidance to cover the mice brain. Source to skin distance of mice on panel was 40 cm. The 10 Gy dose was prescribed at 5 mm depth. A Monte Carlo simulation assessed the effect of attenuation and backscatter from the mice and panel. Irradiation varies from 390 to 398 sec as the dose rate fluctuates, but dose delivered stays constant (<0.1%). Control mice were also anesthetized. Mice were returned to the UK Animal Care Facility following radiation and body weight was measured at 24 h and 48 h. A total of 22 sham mice and 23 IR mice were treated. Blood samples were collected via left ventricle puncture and mice brains were isolated and separated via sagittal dissection.

4.2. Blood samples and isolation of EVs

Isolated blood was allowed to clot at room temperature for 30 min and then was centrifuged at 1,300 g for 15 min to separate the serum, which was then separated into aliquots and stored at −80 °C. EVs were isolated from serum using SmartSEC™ HT EV Isolation System for Serum & Plasma (System Biosciences), which isolates EVs into two different fractions (fractions 1 and 2) using size exclusion chromatography. From the total number of mice used during radiation, a total of 15 sham mice and 16 IR mice were selected for EV isolation. Fraction 2 was used for protein immunoblotting with Jess Protein Simple technology (San Jose, CA, USA) and nanoparticle tracking analysis (NTA); fraction 1 was used for HNE protein adduction measurement. BCA assay from ThermoFisher measured protein concentration.

4.3. Nanoparticle tracking analysis

EVs particle size distribution was determined by NanoSight NS300 (Malvern Panalytical, UK). Fraction 2 of SmartSEC HT isolated EVs were diluted with PBS to achieve particle range of 20–100 particles per frame on an instrument. Specimens were analyzed at 25 °C at camera level 15 and detection threshold level at 4. Five 60-second videos were recorded for each specimen. Each video was analyzed with NTA 3.2 software (Malvern, UK) and data were recorded and analyzed.

4.4. HNE adducted protein measurement

4-hydroxy-2-nonenal protein adductions in mouse serum and EVs isolated from the serum were measured using standardized immunoblots from the Redox Metabolism Shared Resource Facility of the UK Markey Cancer Center. The facility utilizes the previously documented slot-blot method to quantify the number of HNE protein adducts (Aluise et al., 2009). EVs from fraction 1 were lysed with radio-immunoprecipitation assay buffer and protein concentration was measured by BCA assay kit (ThermoFisher). Bands from HNE immunoblotting were documented with Adobe Photoshop and quantified using Scion Image. Band intensities for HNE protein adducts were normalized utilizing sample standards across

multiple blots to compare detected intensities. Samples from 14 mice in each group were used for serum and EV HNE- adducted proteins.

4.5. Protein immunoblotting

EVs or homogenized brain tissue samples were lysed with RIPA buffer and separated by capillary electrophoresis using Jess by Protein Simple © technology (San Jose, CA, USA). The primary GFAP antibody was purchased from Aviva Systems (OAEB01041, 1:20 dilution). The anti-goat secondary antibody used was supplied by Protein Simple. Compass Software analyzed the data. Protein normalization plates were used for EVs samples, and total area under the curve for each peak detected by the responding protein antibody was normalized by the total protein area.

4.6. Immunohistochemistry

Half of the brain was fixed in 4% paraformaldehyde in PBS for 48 h and then in 30% sucrose for staining by the Biospecimen Procurement and Translational Pathology Shared Resource Facility of the Markey Cancer Center. Immunohistochemistry (IHC) staining for GFAP was performed using the Ventana Discovery Ultra Autostainer. The antigen retrieval was set at “cc1 standard” and incubated with the primary antibody (1:2000, Abcam, ab7260) at 37 °C for 1 h prior to detection by Ventana OmniMap HRP and Ventana DAB, according to manufacturer’s recommendations. Ventana Discovery Ultra Autostainer also performed HNE IHC staining, at a “cc2 mild” setting and a horse serum blocking step. The primary antibody for HNE (1:100, Abcam, ab46545) was incubated at room temperature for 1 h prior to detection by Ventana OmniMap HRP and Ventana DAB, according to manufacturer’s recommendations. Following IHC staining, slides were uploaded onto Aperio eSlide Manager and then quantified with HALO software (version 3.2) by Indica Labs. The area quantification algorithm v2.1.7 was used to detect positive staining of the markers indicated; quantity of positive staining in the sham and IR groups was assessed. 5 representative mice from both sham and IR groups were utilized for IHC staining.

4.7. Statistical analysis

Descriptive statistics, including means and standard deviation, that were calculated for each group are represented in bar graphs. Pairwise comparisons of sham vs. IR were performed using two-sample *t*-test for several quantitative endpoints, including EVs protein levels, EVs particle size, AUC of several proteins, HNE, IHC levels. Body weight measurements were repeatedly summarized and compared using linear mixed models to account for repeated measurements of mice. A nonlinear mixed model was employed to determine the association of vesicle count migration as a function of vesicle diameter, treatment group (IR vs. sham) and interaction between these two factors. The vesicle count was modeled as a negative binomial distribution allowing for random effects of intercept across mouse blood samples and separate covariance specifications for each treatment group. Validity of assumptions and equality of variance of parametric tests and models were tested; data were log transformed as necessary. Statistical analyses were performed using SAS version 9.4.

Supplementary Material

Refer to Web version on PubMed Central for supplementary material.

Acknowledgements

The authors would like to acknowledge the Biospecimen Procurement and Translational Pathology Shared Resource Facility (Dana Napier and Dr. Therese Bocklage), the Redox Metabolism Shared Resource Facility (Michael Alstott), and the Biostatistics and Bioinformatics Shared Resource Facility at the Markey Cancer Center.

Funding

This work was supported by the National Institutes of Health (5R01CA217934-04), National Institute of Environmental Health Sciences (T32ES07266), the National Cancer Institute Cancer Center Support Grant (P30 CA177558), the National Institue of General Medical Sciences (P20 P20 GM121327), and the University of Kentucky Center for Clinical and Translational Science (NIH-UL1TR001998).

References

Hall EJ, 1973. Radiobiology for the radiologist Hagerstown, Md. : Medical Dept., Harper & Row, [1973] ©1973.

Vitali M, Ripamonti CI, Roila F, Proto C, Signorelli D, Imbimbo M, Corrao G, Brissa A, Rosaria G, de Braud F, Garassino MC, Lo Russo G, 2017. Cognitive impairment and chemotherapy: a brief overview. Crit. Rev. Oncol. Hematol 118, 7–14. 10.1016/j.critrevonc.2017.08.001. [PubMed: 28917271]

Cheung YT, Sabin ND, Reddick WE, Bhojwani D, Liu W, Brinkman TM, Glass JO, Hwang SN, Srivastava D, Pui C-H, Robison LL, Hudson MM, Krull KR, 2016. Leukoencephalopathy and long-term neurobehavioural, neurocognitive, and brain imaging outcomes in survivors of childhood acute lymphoblastic leukaemia treated with chemotherapy: a longitudinal analysis. Lancet Haematol 3 (10), e456–e466. 10.1016/S2352-3026(16)30110-7. [PubMed: 27658980]

Brinkman TM, Ness KK, Li Z, Huang I-C, Krull KR, Gajjar A, Merchant TE, Klosky JL, Partin RE, Tonning Olsson I, Boop F, Klimo P, Chemaitilly W, Khan RB, Srivastava D, Robison LL, Hudson MM, Armstrong GT, 2018. Attainment of Functional and Social Independence in Adult Survivors of Pediatric CNS Tumors: A Report From the St Jude Lifetime Cohort Study. J. Clin. Oncol 36 (27), 2762–2769. 10.1200/JCO.2018.77.9454. [PubMed: 30091946]

van Niel G, D'Angelo G, Raposo G, 2018. Shedding light on the cell biology of extracellular vesicles. Nat. Rev. Mol. Cell Biol 19 (4), 213–228. 10.1038/nrm.2017.125. [PubMed: 29339798]

EL Andaloussi S, Mäger I, Breakefield XO, Wood MJA, 2013. Extracellular vesicles: biology and emerging therapeutic opportunities. Nat. Rev. Drug Discov 12 (5), 347–357. 10.1038/nrd3978. [PubMed: 23584393]

Shah R, Patel T, Freedman JE, 2018. Circulating Extracellular Vesicles in Human Disease. N. Engl. J. Med 379 (22), 2180–2181. 10.1056/NEJMc1813170.

Melo S, Sugimoto H, O'Connell J, Kato N, Villanueva A, Vidal A, Qiu L.e., Vitkin E, Perelman L, Melo C, Lucci A, Ivan C, Calin G, Kalluri R, 2014. Cancer exosomes perform cell-independent microRNA biogenesis and promote tumorigenesis. Cancer Cell 26 (5), 707–721. 10.1016/j.ccell.2014.09.005. [PubMed: 25446899]

Shao H, Chung J, Balaj L, Charest A, Bigner DD, Carter BS, Hochberg FH, Breakefield XO, Weissleder R, Lee H, 2012. Protein typing of circulating microvesicles allows real-time monitoring of glioblastoma therapy. Nat. Med 18 (12), 1835–1840. 10.1038/nm.2994. [PubMed: 23142818]

Vader P, Mol EA, Pasterkamp G, Schiffelers RM, 2016. Extracellular vesicles for drug delivery. Adv. Drug Deliv. Rev 106, 148–156. 10.1016/j.addr.2016.02.006. [PubMed: 26928656]

Yarana C, Carroll D, Chen J, Chaiswing L, Zhao Y, Noel T, Alstott M, Bae Y, Dressler EV, Moscow JA, Butterfield DA, Zhu H, St. Clair DK, 2018. Extracellular vesicles released by cardiomyocytes in a doxorubicin-induced cardiac injury mouse model contain protein biomarkers of early cardiac injury. Clin. Cancer Res 24 (7), 1644–1653. 10.1158/1078-0432.CCR-17-2046. [PubMed: 29070527]

Dalleau S, Baradat M, Guéraud F, Huc L, 2013. Cell death and diseases related to oxidative stress: 4-hydroxynonenal (HNE) in the balance. Cell Death Differ 20 (12), 1615–1630. 10.1038/cdd.2013.138. [PubMed: 24096871]

Butterfield DA, Halliwell B, 2019. Oxidative stress, dysfunctional glucose metabolism and Alzheimer disease. Nat. Rev. Neurosci 20 (3), 148–160. 10.1038/s41583-019-0132-6. [PubMed: 30737462]

Subramaniam R, Roediger F, Jordan B, Mattson MP, Keller JN, Waeg G, Butterfield DA, 1997. The lipid peroxidation product, 4-hydroxy-2-trans-nonenal, alters the conformation of cortical synaptosomal membrane proteins. J. Neurochem 69 (3), 1161–1169. 10.1046/j.1471-4159.1997.69031161.x. [PubMed: 9282939]

Tomé WA, Gökhan Ş, Brodin NP, Gulinello ME, Heard J, Mehler MF, Guha C, 2015. A mouse model replicating hippocampal sparing cranial irradiation in humans: A tool for identifying new strategies to limit neurocognitive decline. Sci. Rep 5 (1) 10.1038/srep14384.

Baulch JE, Acharya MM, Allen BD, Ru N, Chmielewski NN, Martirosian V, Giedzinski E, Syage A, Park AL, Benke SN, Parihar VK, Limoli CL, 2016. Cranial grafting of stem cell-derived microvesicles improves cognition and reduces neuropathology in the irradiated brain. Proc. Natl. Acad. Sci. U.S.A 113 (17), 4836–4841. 10.1073/pnas.1521668113. [PubMed: 27044087]

Zhang S, et al. , 2018. Intercellular transfer of pathogenic alpha-synuclein by extracellular vesicles is induced by the lipid peroxidation product 4-hydroxynonenal. Neurobiol. Aging 61, 52–65. 10.1016/j.neurobiolaging.2017.09.016. [PubMed: 29035751]

Lovell MA, Markesbery WR, 2007. Oxidative DNA damage in mild cognitive impairment and late-stage Alzheimer's disease. Nucleic Acids Res 35 (22), 7497–7504. 10.1093/nar/gkm821. [PubMed: 17947327]

Sultana R, Butterfield DA, Lovell MA, 2010. Role of oxidative stress in the progression of Alzheimer's disease. J. Alzheimers Dis 19 (1), 341–353. [PubMed: 20061649]

Perluigi M, Coccia R, Butterfield DA, 2012. 4-Hydroxy-2-nonenal, a reactive product of lipid peroxidation, and neurodegenerative diseases: a toxic combination illuminated by redox proteomics studies. Antioxid. Redox Signal 17 (11), 1590–1609. 10.1089/ars.2011.4406. [PubMed: 22114878]

Di Domenico F, Tramutola A, Butterfield DA, 2017. Role of 4-hydroxy-2-nonenal (HNE) in the pathogenesis of alzheimer disease and other selected age-related neurodegenerative disorders. Free Radic. Biol. Med 111, 253–261. 10.1016/j.freeradbiomed.2016.10.490. [PubMed: 27789292]

Chatterjee P, Pedrini S, Stoops E, Goozee K, Villemagne VL, Asih PR, Verberk IMW, Dave P, Taddei K, Sohrabi HR, Zetterberg H, Blennow K, Teunissen CE, Vanderstichele HM, Martins RN, 2021. Plasma glial fibrillary acidic protein is elevated in cognitively normal older adults at risk of Alzheimer's disease. Transl. Psychiatry 11 (1). 10.1038/s41398-020-01137-1.

Middeldorp J, Hol EM, 2011. GFAP in health and disease. Prog. Neurobiol 93 (3), 421–443. 10.1016/j.pneurobio.2011.01.005. [PubMed: 21219963]

Keeney JTR, Ren X, Warrier G, Noel T, Powell DK, Brelsfoard JM, Sultana R, Saatman KE, St. Clair DK, Butterfield DA, 2018. Doxorubicin-induced elevated oxidative stress and neurochemical alterations in brain and cognitive decline: protection by MESNA and insights into mechanisms of chemotherapy-induced cognitive impairment ("chemobrain"). Oncotarget 9 (54), 30324–30339. 10.18632/oncotarget.25718. [PubMed: 30100992]

Hyvarinen T, et al. , 2019. Co-stimulation with IL-1beta and TNF-alpha induces an inflammatory reactive astrocyte phenotype with neurosupportive characteristics in a human pluripotent stem cell model system. Sci. Rep 9 (1), 16944. 10.1038/s41598-019-53414-9. [PubMed: 31729450]

Tangpong J, et al. , 2006. Adriamycin-induced, TNF-alpha-mediated central nervous system toxicity. Neurobiol. Dis 23 (1), 127–139. 10.1016/j.nbd.2006.02.013. [PubMed: 16697651]

Tangpong J, Cole MP, Sultana R, Estus S, Vore M, St. Clair W, Ratanachaiyavong S, St. Clair DK, Butterfield DA, 2007. Adriamycin-mediated nitration of manganese superoxide dismutase in the central nervous system: insight into the mechanism of chemobrain. J. Neurochem 100 (1), 191–201. 10.1111/j.1471-4159.2006.04179.x. [PubMed: 17227439]

Chen Y, Jungsuwadee P, Vore M, Butterfield DA, St. Clair DK, 2007. Collateral damage in cancer chemotherapy: oxidative stress in nontargeted tissues. Mol. Interv 7 (3), 147–156. 10.1124/mi.7.3.6. [PubMed: 17609521]

Aluise CD, et al. , 2011. 2-Mercaptoethane sulfonate prevents doxorubicin-induced plasma protein oxidation and TNF-alpha release: implications for the reactive oxygen species-mediated mechanisms of chemobrain. Free Radic. Biol. Med 50 (11), 1630–1638. 10.1016/j.freeradbiomed.2011.03.009. [PubMed: 21421044]

Sompol P, Ittarat W, Tangpong J, Chen Y, Doubinskaia I, Batinic-Haberle I, Abdul HM, Butterfield DA, St. Clair DK, 2008. A neuronal model of Alzheimer's disease: an insight into the mechanisms of oxidative stress-mediated mitochondrial injury. Neuroscience 153 (1), 120–130. [PubMed: 18353561]

Ma C-M, Coffey CW, DeWerd LA, Liu C, Nath R, Seltzer SM, Seuntjens JP, 2001. AAPM protocol for 40–300 kV x-ray beam dosimetry in radiotherapy and radiobiology. Med. Phys 28 (6), 868–893. 10.1118/1.1374247. [PubMed: 11439485]

Chen Q, Carlton D, Howard TJ, Izumi T, Rong Y.i., 2021. Technical Note: Vendor miscalibration of preclinical orthovoltage irradiator identified through independent output check. Med. Phys 48 (2), 881–889. 10.1002/mp.14642. [PubMed: 33283893]

Aluise CD, St. Clair D, Vore M, Butterfield DA, 2009. In vivo amelioration of adriamycin induced oxidative stress in plasma by gamma-glutamylcysteine ethyl ester (GCEE). Cancer Lett 282 (1), 25–29. 10.1016/j.canlet.2009.02.047. [PubMed: 19342159]

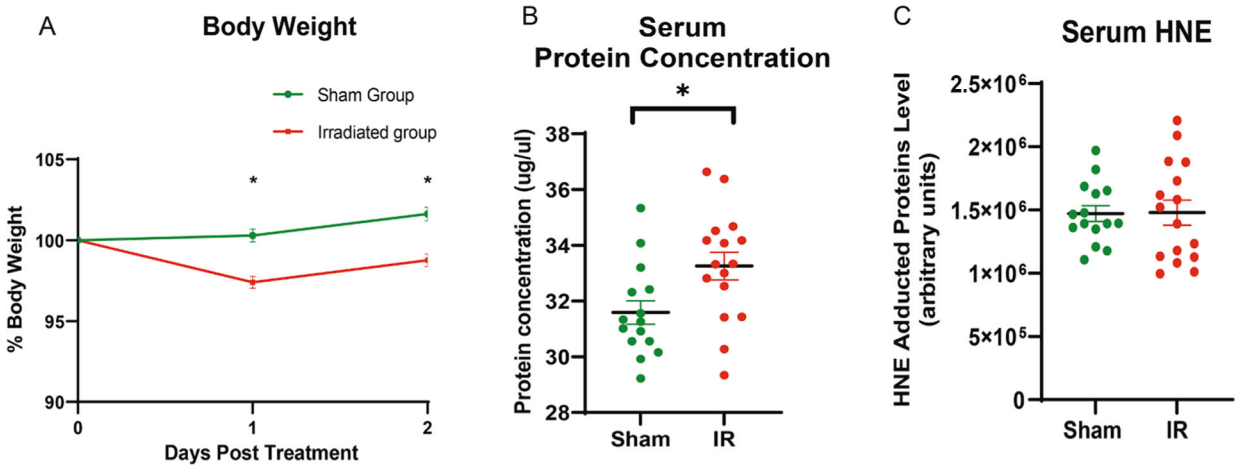

Fig. 1.

Different changes in mice weight and protein concentration were observed in the sham and IR group. (A) Significant change was observed in the mice that received the cranial radiation compared to the sham group ($p < 0.05$). (B) Serum protein levels were elevated in the IR group (red dots) compared to the sham group (green dots) as measured by the BCA assay. (C) The levels of HNE adducted proteins were measured and the differences were not significant in the two groups.

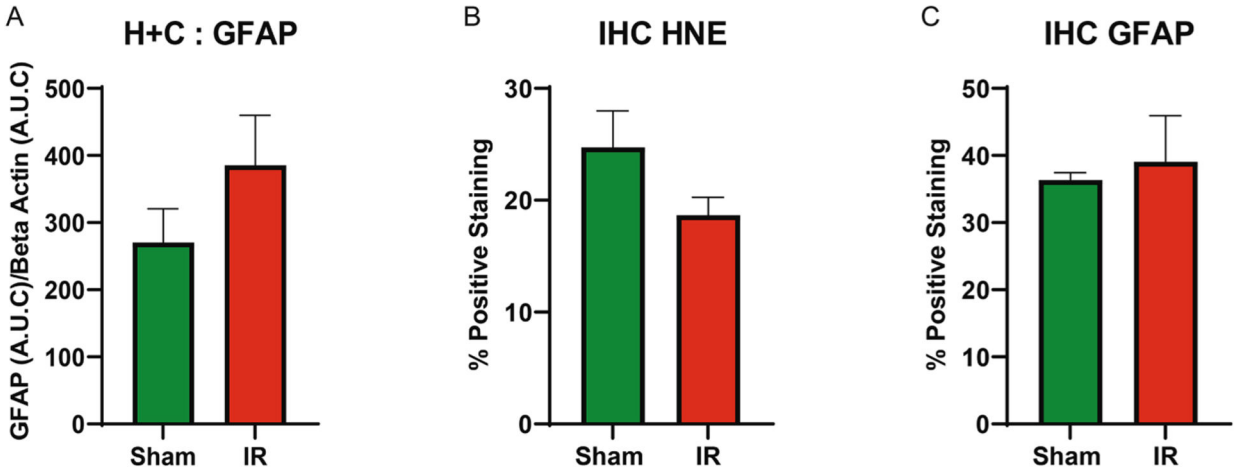

Fig. 2.

IHC staining of brain tissue and brain tissue lysates revealed no observable changes. Probing for GFAP in the brain tissue lysate (A) also revealed no significant differences. Additionally, quantification of IHC staining of HNE (B) and GFAP (C) in the brain tissue resulted in no significant differences.

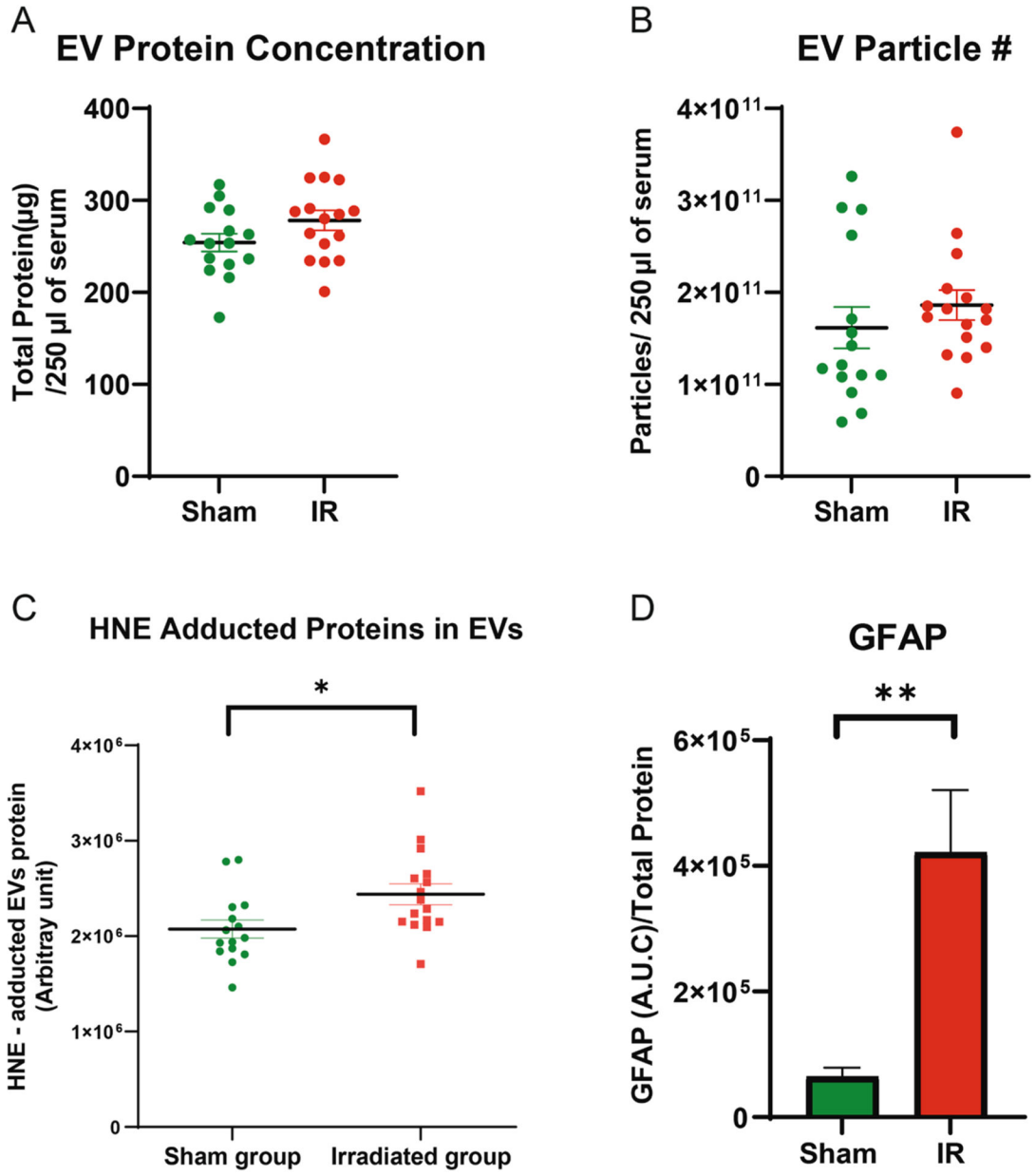

Fig. 3.

Elevated levels of HNE and astrocyte activation were observed in the EVs obtained from the IR mice. The protein concentration (A) and the number of EVs particles (B) appeared to be elevated in the IR mice compared to the sham group, though neither reached statistical significance ($p = 0.059$ and $p = 0.282$, respectively). However, EVs lysates isolated from the IR mice had an increase in HNE adducted proteins (C, $p < 0.05$) and GFAP (D, $p < 0.05$) compared to the sham group.